

Article

Influence of Pipeline Leakage on the Ground Settlement around the Tunnel during Shield Tunneling

Xin Shi ^{1,2} , Yi Cao ¹ , Chuanxin Rong ^{1,2,*}, Gangjian An ³, Houliang Wang ⁴ and Linzhao Cui ⁴

¹ Engineering Research Center of Underground Mine Construction, Ministry of Education, Anhui University of Science and Technology, Huainan 232001, China

² School of Civil Engineering and Architecture, Anhui University of Science and Technology, Huainan 232001, China

³ The Fourth Engineering Co., Ltd. of China Railway No.4 Engineering Group, Hefei 230012, China

⁴ Anhui Construction Engineering Group Co., Ltd., Bengbu 233000, China

* Correspondence: chxrong@aust.edu.cn; Tel.: +86-0554-6668693

Abstract: Shield tunneling is widely used in urban subway tunnel construction. Old urban underground pipelines generally have small leakages that are difficult to find. The water leakage significantly reduces the stability of the stratum, posing a threat to the safety of tunnel shield construction. Therefore, this study established 2D and 3D calculation models for analyzing the law of the leakage diffusion in the ground under water pressure, and the influences of the pipeline leakage range and leakage length on the changes in ground settlement during shield tunneling. The 2D model calculation results show that seepage water mainly diffuses vertically under gravity. As the pipeline leakage gradually reaches a predetermined depth, the simulation results tend to be consistent with the test results. The 3D model is more accurate than the theoretical solution in predicting the ground settlement because it can consider the influences of repeated disturbances in twin tunnel shield construction. The maximum ground surface settlement increases with the extent of the leakage length and leakage range, and the range is the main factor determining the settlement. At the interior of the ground, the seepage water has a greater impact on areas with strong disturbances and large soil losses.

Keywords: shield construction; pipeline leakage; ground settlement; numerical simulation



Citation: Shi, X.; Cao, Y.; Rong, C.; An, G.; Wang, H.; Cui, L. Influence of Pipeline Leakage on the Ground Settlement around the Tunnel during Shield Tunneling. *Sustainability* **2022**, *14*, 16802. <https://doi.org/10.3390/su142416802>

Academic Editors: Hong Wong, Dan Ma, Lang Liu, Jiangyu Wu and Wen Zhong

Received: 1 December 2022

Accepted: 12 December 2022

Published: 14 December 2022

Publisher's Note: MDPI stays neutral with regard to jurisdictional claims in published maps and institutional affiliations.



Copyright: © 2022 by the authors. Licensee MDPI, Basel, Switzerland. This article is an open access article distributed under the terms and conditions of the Creative Commons Attribution (CC BY) license (<https://creativecommons.org/licenses/by/4.0/>).

1. Introduction

As the traffic pressure on urban roads continues to increase, the construction of subway traffic networks is becoming increasingly crucial. Underground pipelines (particularly crisscrossing ones) generally face aging, abrasion, and other problems, and their safety and stability in the construction process of subway tunnels are extremely important. The industry standard stipulates that the basic leakage rate of urban underground pipelines used for water supply and drainage should be less than 12%. This indicates that pipeline leakage is common. In unsaturated ground, seepage water changes the physical and mechanical properties of the soil and increases the pipeline deformation and ground settlement during shield construction. An evaluation of the adverse effects of pipeline leakage and shield construction coupling is therefore of great significance for tunnel construction.

In terms of theoretical research, a two-stage method is widely used to analyze the pipeline responses caused by shield construction, owing to its clear logic and easy solution [1–3]. In addition, many scholars have focused research on the responses of discontinuous pipelines owing to shield tunneling [4–7]. In terms of test research, there are two main deficiencies in the current research. First, most of the test materials are sandy soil [8–13]; research on the influences of seepage water on unsaturated clay is relatively limited. Second, actual tunnel construction is a three-dimensional dynamic process, and most three-dimensional model tests have not yet considered the adverse effects of the

repeated disturbances in the proximity construction of twin tunnels [14,15]. In simulations and the actual measurements of pipeline responses, most scholars have considered the influences of shield construction on the deformation performance of existing underground pipelines [16–23]. However, they have ignored the change(s) in the ground settlement law resulting from the construction disturbance under pipeline leakages.

Therefore, based on the tunnel project of Hefei Rail Transit Line 4, in China, this study established two-dimensional and three-dimensional finite element calculation models. The two-dimensional model was used to analyze the seepage diffusion law in the plane under the action of water pressure. Based on this, a three-dimensional finite element calculation model was constructed for the one-way coupling between the shield tunneling and pipeline leakage. The rationality of the model was verified by comparing the results from previous model tests and theoretical calculations. Finally, further consideration was given to the influences of: (a) the diffusion range of the pipeline leakage water along the depth direction; and (b) the length of the leakage section along the pipeline length direction on the changes in the stratum displacement. This study can provide a reference for predicting and evaluating the risk of shield construction in leakage pipelines.

2. Project Overview

This project consisted of two straight tunnels constructed near the station foundation pit using the shield method. The distance between the centerlines of the two tunnels was 15 m, and the buried depth of the tunnel center was 15 m. The excavation direction of the tunnel was perpendicular to the pipeline trend. Before excavation, the pipeline was found to have a long-term leakage based on drilling. The leakage was small, but a certain diffusion range had formed in the ground. The maximum buried depth of the pipeline center was 6 m. The relative positional relationship between the tunnel and pipeline is shown in Figure 1. The tunnel and pipeline were both in an unsaturated clay stratum. The relevant parameters of the pipeline and soil are listed in Table 1.

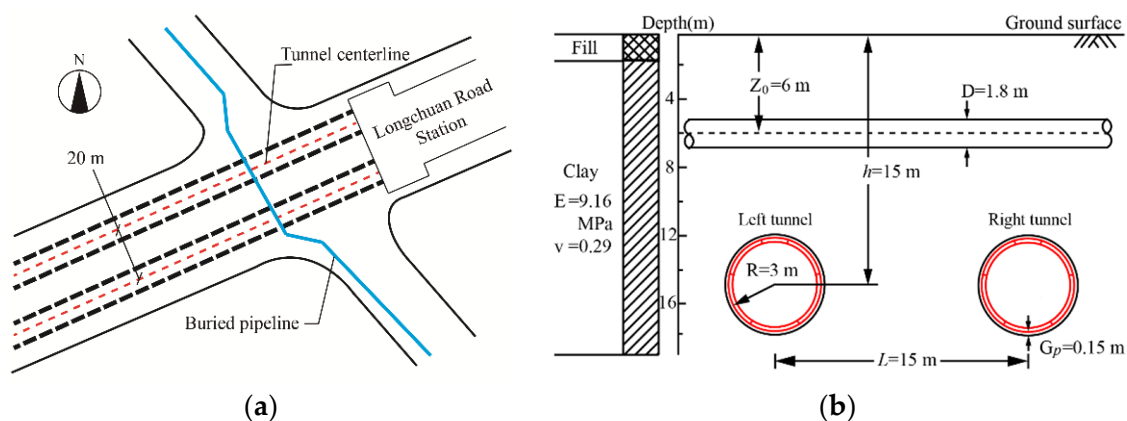


Figure 1. Layout of measuring points and relative position relationship between tunnel and pipeline: (a) Plan view; (b) section and layout of measuring points.

Table 1. Calculation parameters of pipeline and soil.

Tunnel Radius R/m	Buried Depth of Tunnel h/m	Burial Depth of Pipeline Z_0/m	Outer Diameter of Pipeline D/m	Pipeline Thickness d/m	Pipeline Stiffness $E_p I_p / (kN \cdot m^2)$	Elastic Modulus of Soil E/MPa	Poisson's Ratio of Soil ν	Soil Loss Rate ϵ_0
3	15	6	1.8	0.18	1.82×10^7	9.16	0.29	0.0184

There were six strata within the scope of the project where the tunnel was located. From top to bottom, they were silty clay, hard clay, medium clay, completely weathered

sandy mudstone, strongly weathered sandy mudstone, and moderately weathered sandy mudstone. Their basic physical and mechanical parameters are presented in Table 2.

Table 2. Basic physical and mechanical parameters of soil.

Soil Name	γ : kN/m ³	C' : kPa	Φ' : Degrees	K_0	E_S : MPa
Fill	18.8	10	8	0.65	8
Medium clay	19.5	55	14	0.39	12
Stiff clay	19.9	36	16	0.38	13
Fully weathered sandy mudstone	19.0	35	18	0.38	-
Strongly weathered sandy mudstone	21.3	45	20	0.32	27.86
Moderately weathered sandy mudstone	21.7	50	25	-	33.64

3. Numerical Simulation

3.1. Simulation Analysis of Pipeline Leakage Diffusion

To study the seepage diffusion law of the pipeline under the action of water pressure, ABAQUS was used to establish a two-dimensional numerical calculation model for the plane strain. The results from the model grid division are shown in Figure 2. The length and height of the model were 30 and 15 m, respectively, and the buried depth of the pipeline centerline was 6 m, consistent with the actual working conditions. The overall model was divided into 3600 units. The seepage coupling unit CPE4P was used for the soil, and a plane strain unit was used for the pipeline.

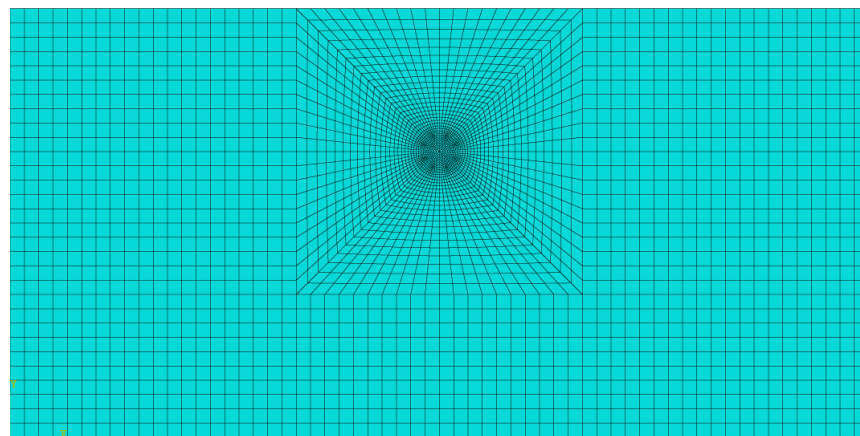


Figure 2. Model meshing diagram.

When conducting a fluid–solid coupling analysis for an unsaturated formation, it is necessary to define the relationships among the unsaturated soil permeability coefficient, matrix suction, and saturation. According to indoor test results on the unsaturated clay's permeability suction and matrix suction, as shown in Figure 3, the stress parameter values can be obtained by combining Equations (1) and (2). The test process is described in detail in the literature [24].

$$K_w = \frac{a_w K_{ws}}{[a_w + (b_w \times (u_a - u_w))^{c_w}]^2} \quad (1)$$

$$S_r = \frac{S_i + (S_n - S_i)a_s}{[a_s + (b_s \times (u_a - u_w))^{c_s}]^2} \quad (2)$$

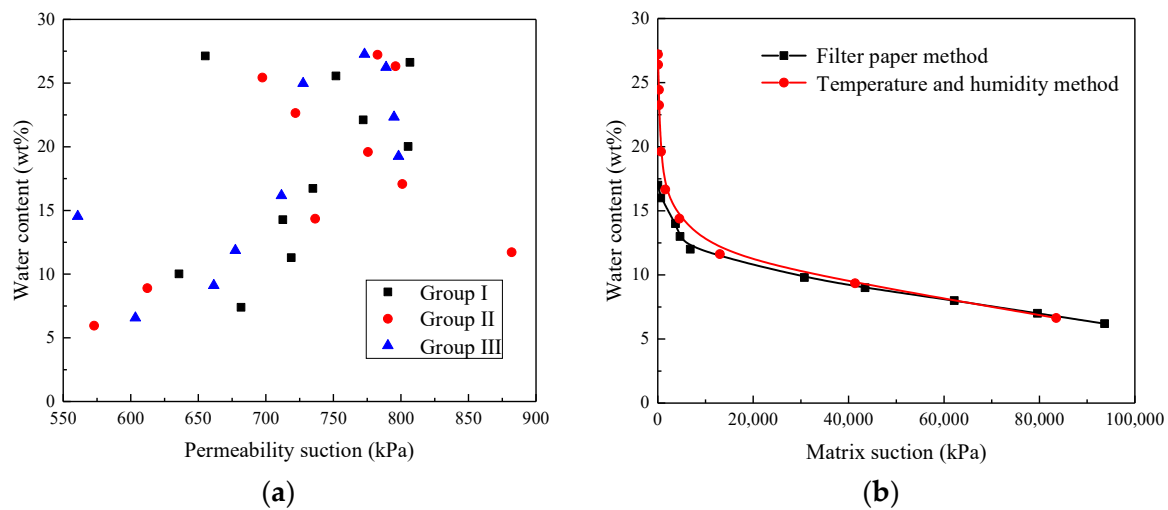


Figure 3. Laboratory test results of soil suction: (a) permeability suction; (b) Matrix suction.

In the above, K_w is the permeability coefficient; K_{ws} is the permeability coefficient of the soil in the saturated state; u_a is the air pressure in the soil mass, and is assumed to be 0; u_w is the water pressure in the soil mass; S_r is the saturation; S_n is the maximum saturation, and the value is 1; S_i is the residual saturation; $a_w, b_w, c_w, a_s, b_s, c_s$ are material coefficients, and their values are 1000, 0.01, 1.7, 1.5×10^{-5} , and 3.5, respectively.

To conduct a seepage analysis on unsaturated soil, the initial stress distribution, initial pore pressure, initial saturation, initial void ratio, and other conditions must be set. Table 3 presents the settings in this study.

Table 3. Setting of model initial conditions.

Type	Initial Stress Distribution	Initial Pore Pressure (kPa)	Initial Saturation	Initial Void Ratio
3	15	6	1.8	0.18

The model boundary conditions mainly included the displacement and seepage boundaries. For the two-dimensional plane model, the displacement boundary conditions mainly constrained the horizontal and vertical displacements at the bottom of the model and horizontal displacements on both sides of the model. The seepage boundary conditions mainly set the model's permeable seepage boundary. The top and both sides of the model used a permeable boundary, whereas the bottom used an impermeable boundary. In addition, assuming the pipe pressure remained constant, a fixed pore pressure boundary was set at the leakage points on both sides of the pipe bottom.

Figure 4 shows the calculation results regarding the formation saturation distribution during pipeline leakage. It shows that under the initial leakage state of the pipeline, the soil mass at the leakage points on both sides of the pipeline bottom initially reaches the saturation state and is symmetrically distributed. Under the effect of the pipeline pressure, the saturated area near the leakage point is larger, exhibiting a crescent shape. The soil saturation gradually decreases with an increase in the distance from the leakage point. In the initial leakage state of the pipeline, the leakage water mainly diffuses in the horizontal direction and most of the top and surrounding areas of the pipeline remain unsaturated, indicating that a short leakage time cannot cause the soil mass to reach the saturated state in a large area. Therefore, the initial leakage of a pipeline in the early stage of an actual project is usually difficult to detect.

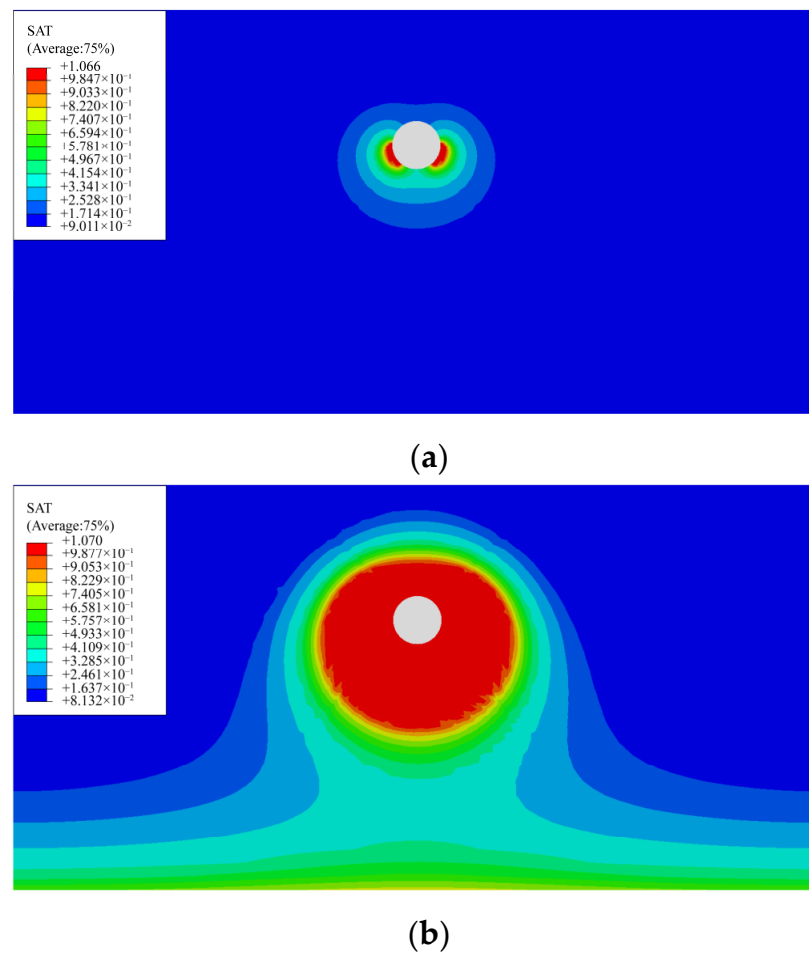


Figure 4. Calculation results of pipeline leakage water diffusion: (a) initial diffusion state; (b) final diffusion state.

With an increase in the leakage time, the soil around the pipeline in a large area reaches the saturation state. The leakage water mainly diffuses vertically under the action of gravity. The final diffusion area of the leakage water exhibits a “heart shape” as a whole. As the boundary condition at the bottom of the model was set as an undrained boundary, the pipeline leakage water discharged from the boundary on both sides after converging at the bottom of the model.

In a previous study, an indoor model test was used to explore the diffusion law of leakage water under the action of water pressure [25]. In combination with Yin Zhong-ping’s [26] experiment on an unsaturated soil dehumidification process, soil color images under different water contents were taken, and the digital information of the soil colors was extracted using MATLAB digital image recognition technology. The relationship between the soil color and matrix suction was established by considering the soil saturation as an intermediate variable. This study uses the same approach to compare the model test calculation results with the numerical simulation results and to analyze the pipe leakage water diffusion law, as shown in Figure 5.

As shown in Figure 5a, in the initial stage of pipeline leakage, the diffusion range of the leakage water in the test is approximately twice of the simulation result. This phenomenon is attributed to the fact that the water in the test diffuses at the interface between the pipe and glass. The diffusion range observed in the test only represents the interface diffusion, which is significantly higher than the diffusion range of the water in the ground layer as calculated by the numerical simulation.

As the pipeline leakage gradually reaches the predetermined depth, as shown in Figure 5b, the diffusion range of the leakage water as obtained by the numerical simulation

tends to be consistent with the test results. However, the simulation results are larger than the test results in a part of the area at the top of the pipeline. This is because, in the simulation, the soil mass is assumed to be homogeneous continuous medium, whereas, in the actual test, there is a macropore structure in the soil mass. The results are partly owing to the presence of the natural pore structure in soil, and partly owing to the difficulty in ensuring uniformity when filling the soil in the test. The existence of pores makes the seepage water spread more smoothly to the bottom of the pipeline under gravity, so the deviation at the top of the pipeline is relatively large.

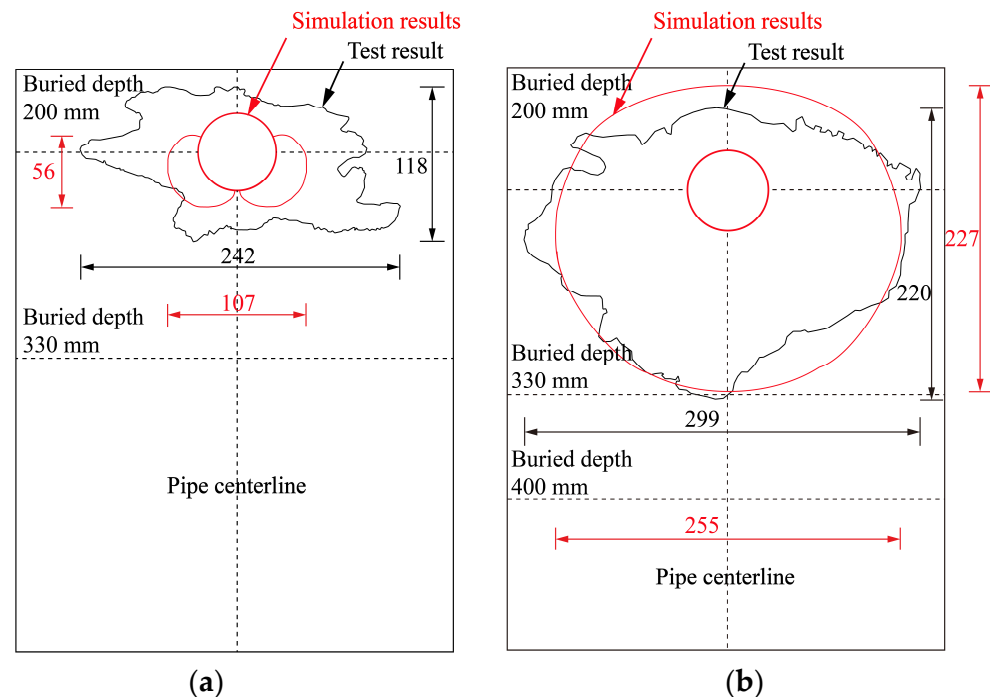


Figure 5. Comparison between simulated and measured results of pipeline leakage diffusion (unit: mm): (a) initial diffusion state; (b) final diffusion state.

3.2. Establishment of Shield Construction Model under Pipeline Leakage

The pipeline leakage was further considered using a three-dimensional shield construction model based on the research on the two-dimensional leakage process. To eliminate the influences of the boundary effect on ground settlement and pipeline deformation caused by the shield construction, the length, width, and height of the model were set to 100, 60, and 50 m. The left and right tunnels in the model each contained 40 segments. Considering the calculation time and accuracy, the grid size of the shield excavation area was 1 m, whereas the model boundary adopted a thicker grid size of approximately 3 m. As the pipeline and leakage area significantly impact the model calculation results, it was necessary to conduct a densification treatment, and the unit size was taken as 0.5 m. The overall model included 76,325 nodes and 144,367 units. The soil mass and grouting area were simulated by solid elements, and the shield shell, lining segment, and underground pipeline were simulated by two-dimensional plate elements, as shown in Figure 6.

To rebuild the real process of the shield construction, the shield thrust gradually moves to the grid node of the next excavation face with the excavation step when the pressure of the previous excavation face is cancelled. The force from the cylinder thrust is applied to the side node of the segment in the form of a line load. When a ring segment has assembled, the force is applied immediately, and the force from the cylinder thrust of the previous ring segment is cancelled to simulate the continuous forwards movement of the cylinder thrust. As the grouting slurry fills in the gap outside the segment and within the outer profile of the excavation surface, the grouting pressure is the surface load applying on the

outermost side of the segment. As the excavation face moves forwards, grouting pressure is applied immediately after segments assembly to simulate synchronous grouting during shield construction. In this study, the shield excavation process is simulated by applying and cancelling the above mentioned loads.

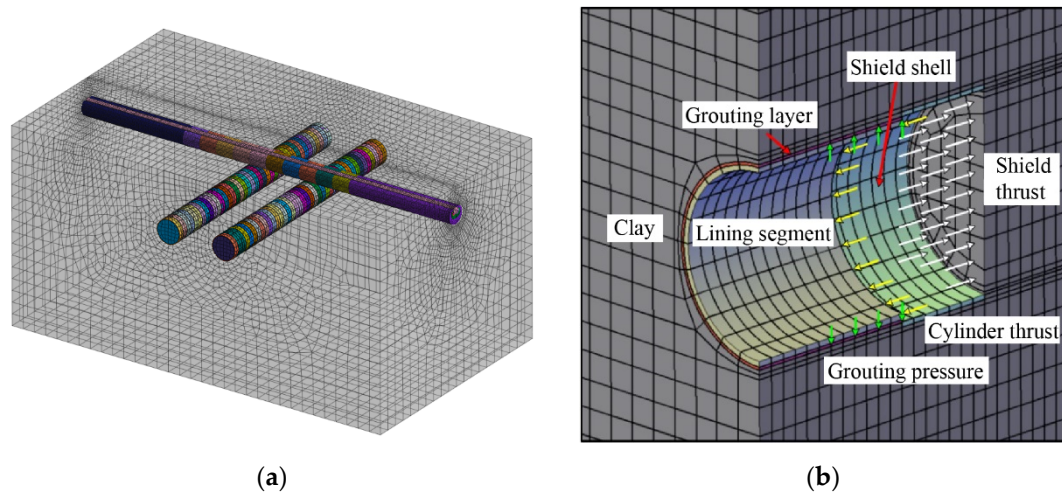


Figure 6. 3D finite element model of pipeline leakage and tunnel excavation: (a) mesh generation of 3D model; (b) simulation of shield construction.

In Zhang Chengping's [27] definition of a pipeline leakage range, a small pipeline leakage is defined as the lowest point of the leakage range extending to the midpoint of the pipeline bottom and tunnel top. To analyze the influences of different ranges and lengths of leakage sections, the diffusion range and diffusion length of the leakage water were further refined in the model. The diffusion range was divided into small, medium, and large ranges. The medium range referred to the pipeline leakage reaching the tunnel vault, whereas a large range referred to the pipeline leakage reaching the tunnel floor. The diffusion lengths were divided into 9, 27, and 45 m, as shown in Figure 7.

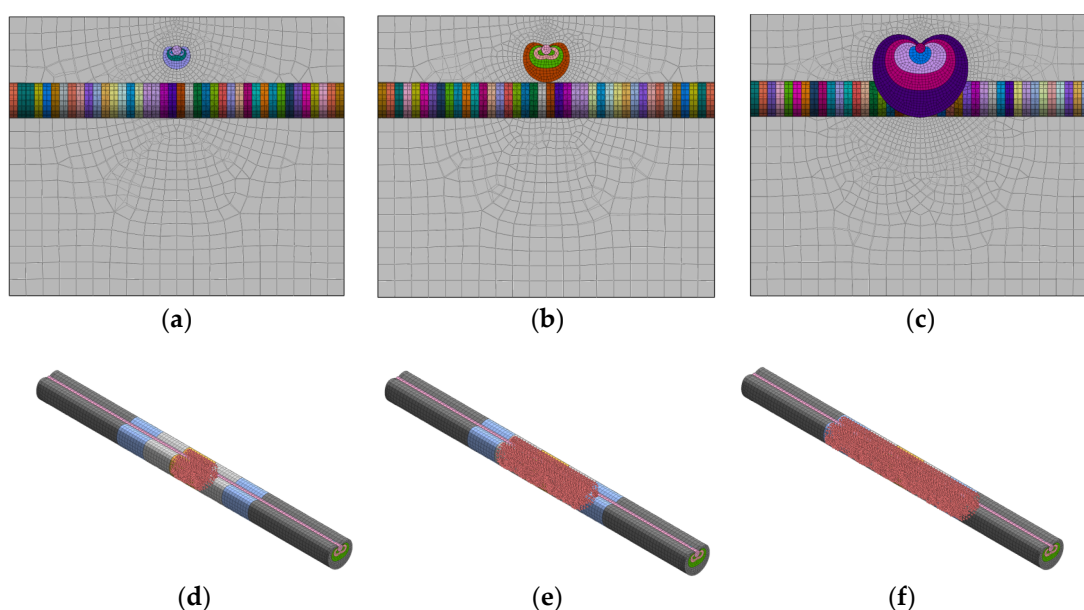


Figure 7. Numerical simulation conditions of different leakage ranges and leakage lengths: (a) small range; (b) medium range; (c) large range; (d) 9 m; (e) 27 m; (f) 45 m.

It is generally believed that the weakening effect from a pipeline leakage on a soil mass between pipes and tunnels mainly reduces the shear strength of the soil mass. In this study, the change in the shear strength index was the main influencing factor in the numerical simulation, while ignoring the influences of other secondary factors. Based on the direct shear test results of soils with different water contents [24], a functional relationship between the saturation and soil shear strength was established to calculate the formation settlement and pipeline deformation caused by a pipeline leakage. The changes in the shear strength index with saturation are listed in Table 4.

Table 4. Corresponding relationship between shear strength parameters and saturation.

Shear Strength Parameters	Saturation							
	30%	40%	50%	60%	70%	80%	90%	100%
C/kPa	11.81	32.13	65.51	72.24	62.33	45.23	29.59	14.21
$\varphi/(\circ)$	32.5	29.27	26	22.72	19.45	16.18	12.91	9.64

3.3. Determination of Parameters

Considering the complexity of pipeline leakage diffusion in actual conditions, the following assumptions were made for the calculation model. The stratum was considered to be homogeneous and isotropic. The soil was unsaturated and the groundwater level was low, so the influence of groundwater was not considered. In the processes of the pipeline leakage and twin tunnel excavation, the internal pressure of the pipeline was a fixed value; and in the numerical simulation, it was assumed that the soil followed a hardened soil model (HS model). The HS model parameters of typical strata in the Hefei area from a previous study [28] were used for the numerical simulation and are listed in Table 5.

Table 5. Hardened soil model (HS model) parameters of the stratum.

Parameters	Unit	Fill	Medium Clay	Stiff Clay	Strongly Weathered Sandy Mudstone	Moderately Weathered Sandy Mudstone
γ_{unsat}	kN/m ³	18.8	19.5	19.9	21.3	21.7
γ_{sat}	kN/m ³	18.8	19.5	19.9	21.3	21.7
C'	kN/m ²	10	55	36	45	50
φ'	\circ	8	14	16	20	25
K_0	-	0.65	0.39	0.38	0.32	0.30
ψ	\circ	0	0	0	0	0
E_{50}^{ref}	kN/m ²	8054	12,167	13,286	27,860	33,640
E_{oed}^{ref}	kN/m ²	8054	12,167	13,286	27,860	33,640
m	-	0.8	0.8	0.8	0.5	0.5
E_{ur}^{ref}	kN/m ²	24,162	36,501	39,858	83,580	100,920
ν_{ur}	-	0.2	0.2	0.2	0.2	0.2
p^{ref}	kN/m ²	100	100	100	100	100
R_f	-	0.9	0.9	0.9	0.9	0.9
E_S	kN/m ²	8054	12,167	13,286	27,860	33,640
e_0	-	0.8	0.7	0.6	0.5	0.5

4. Rationality Verification of the Model

It is necessary to verify the applicability of the three-dimensional finite element model, particularly considering that most of the existing studies do not consider the impacts of pipeline leakages. In addition, the analytical solution generally has high accuracy and is in good agreement with the actual working conditions. Therefore, first, an analytical study was conducted under the condition that the pipeline does not leak. Then, the results

from the analytical solution were compared with the numerical simulation results from this study, so as to verify the reliability of this model for the analysis of shield construction.

4.1. Analytical Study on Ground Settlement Caused by Shield Construction Considering Multiple Factors

From the present research [29], the factors influencing the ground settlement caused by shield construction can be summarized into four parts: the additional thrust P_1 of the excavation face, friction P_2 between the shield shell and soil, grouting pressure P_3 , and ground loss V_{loss} . The ground settlement caused by various factors can be expressed as follows.

The additional thrust of excavation face P_1 is calculated as follows:

$$\bar{v}_1(t) = \int_0^{2\pi} \int_0^R \frac{P_{1l}x_{1l}y_{1l}}{16\pi} \left[\left(\frac{1}{M^3} - \frac{6zh_{1l}}{N^5} \right) a_1 + \frac{1}{N^3} a_2 - \frac{4}{N(N+z+h_{1l})^2} a_3 \right] r dr d\theta + \int_0^{2\pi} \int_0^R \frac{P_{1r}x_{1r}y_{1r}}{16\pi} \left[\left(\frac{1}{M^3} - \frac{6zh_{1r}}{N^5} \right) a_1 + \frac{1}{N^3} a_2 - \frac{4}{N(N+z+h_{1r})^2} a_3 \right] r dr d\theta \quad (3)$$

$$\bar{w}_1(t) = \int_0^{2\pi} \int_0^R \frac{P_{1l}x_{1l}}{16\pi} \left[\left(\frac{z-h_{1l}}{M^3} - \frac{6zh_{1l}(z+h_{1l})}{N^5} \right) a_1 + \frac{z-h_{1l}}{N^3} a_2 - \frac{4}{N(N+z+h_{1l})} a_3 \right] r dr d\theta + \int_0^{2\pi} \int_0^R \frac{P_{1r}x_{1r}}{16\pi} \left[\left(\frac{z-h_{1r}}{M^3} - \frac{6zh_{1r}(z+h_{1r})}{N^5} \right) a_1 + \frac{z-h_{1r}}{N^3} a_2 - \frac{4}{N(N+z+h_{1r})} a_3 \right] r dr d\theta \quad (4)$$

The friction between the shield shell and soil P_2 is calculated as follows:

$$\bar{v}_2(t) = \int_0^{2\pi} \int_0^J \frac{P_{2l}x_{2l}y_{2l}}{16\pi} \left[\left(\frac{1}{M^3} - \frac{6zh_{2l}}{N^5} \right) a_1 + \frac{1}{N^3} a_2 - \frac{4}{N(N+z+h_{2l})^2} a_3 \right] R dj d\theta + \int_0^{2\pi} \int_0^J \frac{P_{2r}x_{2r}y_{2r}}{16\pi} \left[\left(\frac{1}{M^3} - \frac{6zh_{2r}}{N^5} \right) a_1 + \frac{1}{N^3} a_2 - \frac{4}{N(N+z+h_{2r})^2} a_3 \right] R dj d\theta \quad (5)$$

$$\bar{w}_2(t) = \int_0^{2\pi} \int_0^J \frac{P_{2l}x_{2l}}{16\pi} \left[\left(\frac{z-h_{2l}}{M^3} - \frac{6zh_{2l}(z+h_{2l})}{N^5} \right) a_1 + \frac{z-h_{2l}}{N^3} a_2 + \frac{4}{N(N+z+h_{2l})} a_3 \right] R dj d\theta + \int_0^{2\pi} \int_0^J \frac{P_{2r}x_{2r}}{16\pi} \left[\left(\frac{z-h_{2r}}{M^3} - \frac{6zh_{2r}(z+h_{2r})}{N^5} \right) a_1 + \frac{z-h_{2r}}{N^3} a_2 + \frac{4}{N(N+z+h_{2r})} a_3 \right] R dj d\theta \quad (6)$$

The grouting pressure P_3 is calculated as follows:

$$\bar{v}_3(x, y, z, t) = \bar{v}_{3l}(x, y, z, t) + \bar{v}_{3r}(x, y, z, t) \quad (7)$$

$$\bar{w}_3(x, y, z, t) = \bar{w}_{3l}(x, y, z, t) + \bar{w}_{3r}(x, y, z, t) \quad (8)$$

The ground loss V_{loss} is calculated as follows:

$$v_4(x, y, z) = v_{4l}(x, y, z) + v_{4r}(x, y, z) = \frac{-R^2(y+L/2+b)}{2} \cdot \frac{h}{h+d_l} \cdot \left\{ \frac{1}{(y+L/2+b)^2+(h-z)^2} + \frac{1}{(y+L/2+b)^2+(h+z)^2} - \frac{4z(h+z)}{[(y+L/2+b)^2+(h+z)^2]^2} \right\} \cdot \frac{4Rg_l(x)-g_l^2(x)}{4R^2} B_l(x) \cdot \exp \left[\frac{(y+L/2+b)^2 \ln \lambda_l(x)}{(h+R)^2} + \frac{z^2(\ln \lambda_l(x) - \ln \delta_l(x))}{(h+d_l)^2} \right] + \frac{-R^2(y-L/2)}{2} \cdot \frac{h}{h+d_r} \cdot \left\{ \frac{1}{(y-L/2)^2+(h-z)^2} + \frac{1}{(y-L/2)^2+(h+z)^2} - \frac{4z(h+z)}{[(y-L/2)^2+(h+z)^2]^2} \right\} \cdot \frac{4Rg_r(x)-g_r^2(x)}{4R^2} B_r(x) \cdot \exp \left[\frac{(y-L/2)^2 \ln \lambda_r(x)}{(h+R)^2} + \frac{z^2(\ln \lambda_r(x) - \ln \delta_r(x))}{(h+d_r)^2} \right] \quad (9)$$

$$\begin{aligned}
 w_4(x, y, z) &= w_{4l}(x, y, z) + w_{4r}(x, y, z) \\
 &= \frac{R^2}{2} \left\{ \frac{h-z}{(y+L/2+b)^2+(h-z)^2} + \frac{h+z}{(y+L/2+b)^2+(h+z)^2} - \frac{2z[(y+L/2+b)^2-(h+z)^2]}{[(y+L/2+b)^2+(h+z)^2]^2} \right\} \cdot \\
 &\quad \frac{4Rg_l(x)-g_l^2(x)}{4R^2} B_l(x) \cdot \exp \left[\frac{(y+L/2+b) \ln \lambda_l(x)}{(h+R)^2} + \frac{z^2(\ln \lambda_l(x)-\ln \delta_l(x))}{(h+d_l)^2} \right] \\
 &\quad \frac{R^2}{2} \left\{ \frac{h-z}{(y-L/2)^2+(h-z)^2} + \frac{h+z}{(y-L/2)^2+(h+z)^2} - \frac{2z[(y-L/2)^2-(h+z)^2]}{[(y-L/2)^2+(h+z)^2]^2} \right\} \cdot \\
 &\quad \frac{4Rg_r(x)-g_r^2(x)}{4R^2} B_r(x) \cdot \exp \left[\frac{(y-L/2) \ln \lambda_r(x)}{(h+R)^2} + \frac{z^2(\ln \lambda_r(x)-\ln \delta_r(x))}{(h+d_r)^2} \right]
 \end{aligned} \tag{10}$$

The relevant parameter definitions can be found in a previous study [30]. The total displacement can be obtained by the superposition of the horizontal and vertical displacements of the stratum owing to the above four factors, as follows:

$$v(x, y, z, t) = \bar{v}_1(x, y, z, t) + \bar{v}_2(x, y, z, t) + \bar{v}_3(x, y, z, t) + v_4(x, y, z) \tag{11}$$

$$w(x, y, z, t) = \bar{w}_1(x, y, z, t) + \bar{w}_2(x, y, z, t) + \bar{w}_3(x, y, z, t) + w_4(x, y, z) \tag{12}$$

4.2. Comparison between Theoretical Analysis and Simulation Results without Leakage

To facilitate analysis of the calculation results, the layout of the measuring points in the calculation model is shown in Figure 8.

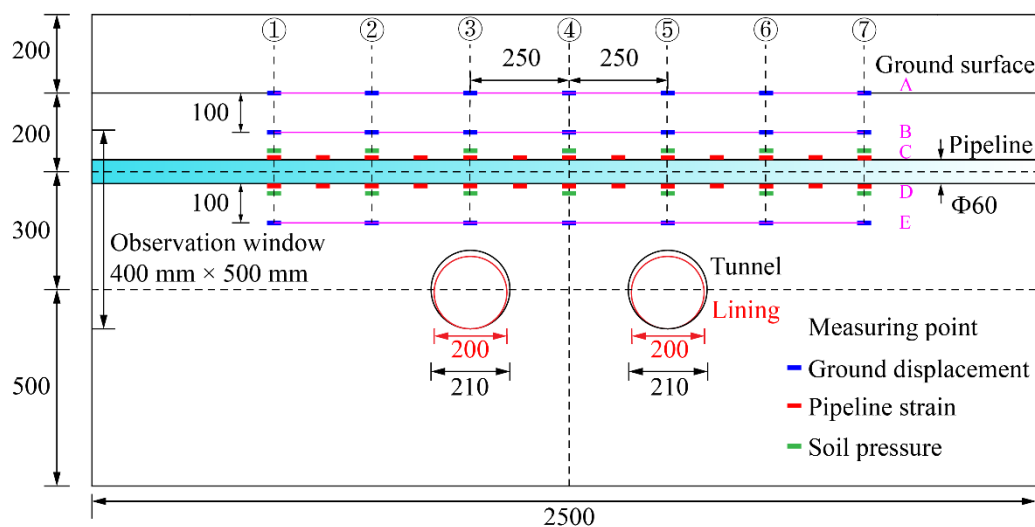


Figure 8. Layout of monitoring points.

With no leakage from the pipeline, the vertical displacement of the stratum obtained by the simulation calculation after the left line tunnel is shown in Figure 9. The figure shows that after the left line tunnel is completed, the maximum ground settlement occurs at the arch crown of the left line tunnel, with a settlement value of 21.4 mm. Under the influence of excavation unloading, the tunnel floor heaves with the amount of 25.9 mm. The settlement value directly above the left line tunnel at the surface is the largest. With an increase in the distance from the tunnel centerline, the settlement value caused by the excavation gradually decreases.

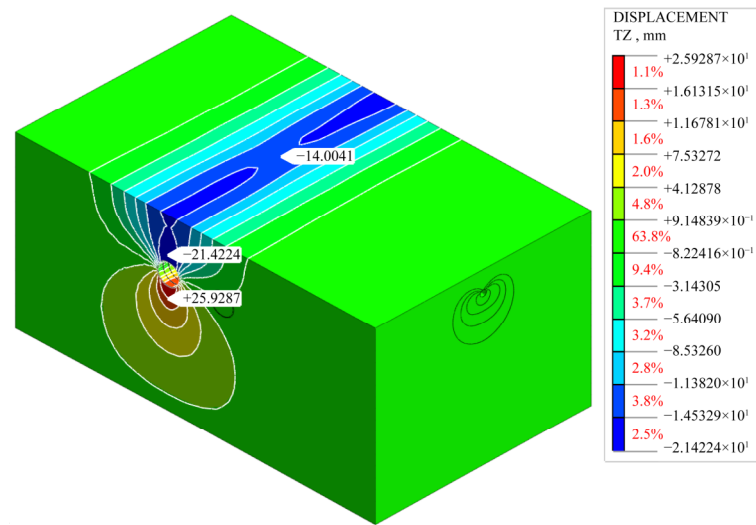


Figure 9. Calculation results of ground vertical displacement after the excavation of the left line tunnel.

The surface unit node A3 above the left line tunnel of the model stratum centerline, surface node A4 above the two tunnel centerlines, and surface node A5 above the right line tunnel are considered, as shown in Figure 8. Based on the present research [25], similar model tests are conducted on the coupling effects of the shield tunneling and pipeline leakage. The vertical displacement change curves of the three monitoring points during the excavation of the left line tunnel are drawn and compared with the theoretical analysis and test results, as shown in Figure 10.

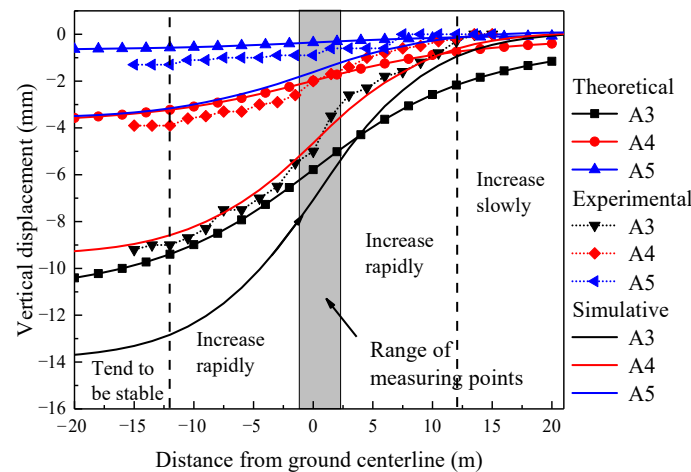


Figure 10. Comparison of theoretical analysis, test, and simulation results of ground vertical displacement after excavation of left tunnel without leakage.

Figure 10 shows that the surface settlement curves obtained from the simulation results, test results, and theoretical analysis, conform to the three-stage change trend. At the initial stage of shield tunneling, the ground settlement of the stratum center increases slowly. As the horizontal distance between the excavation face and stratum center decreases, the ground settlement increases rapidly. When the shield passes through the range of measuring points and exceeds the area affected by the excavation disturbance, the settlement value at the measuring point gradually stabilized. The surface settlement values obtained by the numerical simulation are higher than the test results, and the deviations between the simulation values and test values at the stability stage at the A3, A4, and A5 measuring points are 4.5, 5.4, and 2.2 mm, respectively. The factors causing these deviations can be divided into two aspects. First, the uneven surface pressure distribution of the

model in the test process decreases the surface settlement value. Second, because certain material parameters in the numerical simulation adopt empirical values, the simulation results also have certain deviations.

Figure 11 shows the calculation results for the ground vertical displacement after the twin tunnel is completed without leakage. It shows that the maximum settlement and uplift value points of the twin tunnel still appear at the arch crown and bottom plate of the left line tunnel after the tunnel is completed. Compared with Figure 9, the settlement and uplift values increase slightly, consistent with the conclusions from the model test. This shows that the displacement field generated by twin tunnel excavation is not a simple superposition of the displacement fields generated by single-tunnel excavations. At this interval, the repeated disturbance of the right tunnel excavation still impacts the distribution of the displacement field at the axis of the left tunnel. The settlement of the stratum center after the excavation of the twin tunnel is 18 mm, i.e., evidently increased relative to the case in the completion of the left line construction.

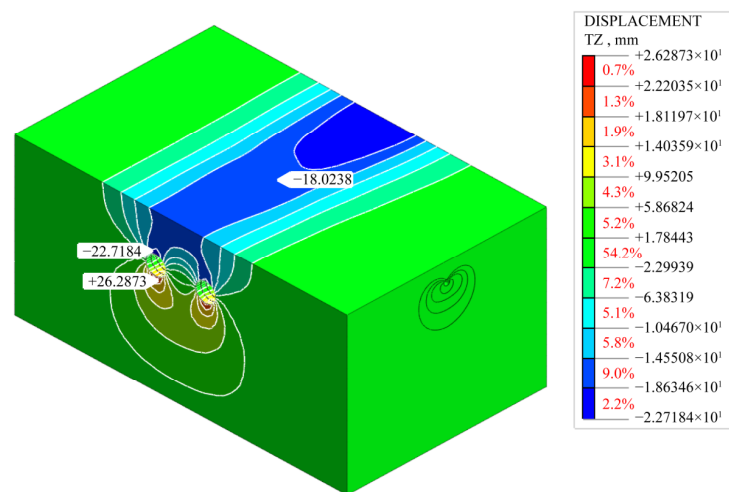


Figure 11. Calculation results of ground vertical displacement after excavation of twin tunnel.

The A3, A4, and A5 nodes of the model are used to draw the vertical displacement change curve of the three nodes during the excavation of the right line tunnel for comparison with the theoretical analysis and test results, as shown in Figure 12.

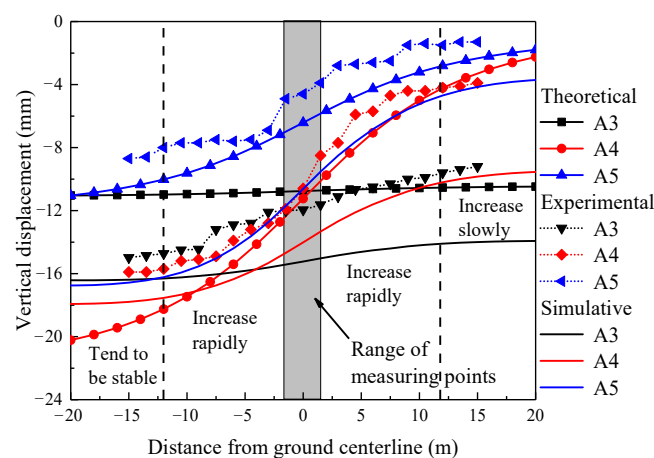


Figure 12. Comparison of theoretical analysis, test, and simulation results of ground vertical displacement after excavation of twin tunnel without leakage.

Figures 9–12 show that, compared with the test results, the prediction of the theoretical solution for the excavation of a single tunnel is more accurate. Whereas, for the excavation

of the twin tunnel, the formation process of the displacement field is more complex. For example, the prediction deviation of the theoretical solution is relatively large. The numerical simulation can consider the impact of repeated disturbances in the shield construction of a twin tunnel, and the prediction is more accurate.

5. Analysis of Influence of Pipeline Leakage Diffusion Range and Leakage Length Change Rule of Ground Displacement under the Influence of Pipeline Leakage

Based on the rationality verification of the three-dimensional model, further consideration was given to the influences of: (a) the diffusion range of the pipeline leakage water along the depth direction; and (b) the length of the leakage section along the pipeline length direction on the changes in the stratum displacement. Nine numerical simulation conditions were established, as listed in Table 6.

Table 6. Numerical simulation condition Nos. of different pipeline leakage ranges and lengths.

Leakage Range	Leakage Length		
	9 m	27 m	45 m
Small range	1	2	3
Medium range	4	5	6
Large range	7	8	9

In the numerical simulation analysis steps, the pipeline began to leak after the initial geostress was balanced. After the seepage diffusion range and diffusion length reached the set values for the corresponding working conditions, the left line tunnel was excavated first, and the right line tunnel was excavated again after the excavation of the left line tunnel was completed. This section analyzes the change rule of the stratum displacement in this order.

Using the overall coordinate system in the model, the pipeline length direction was set as the X-axis, tunnel excavation direction was set as the Y-axis, and stratum depth direction was set as the Z-axis. Figure 13 shows the numerical simulation results for the surface settlement when the leakage was completed under different working conditions (Z axis direction).

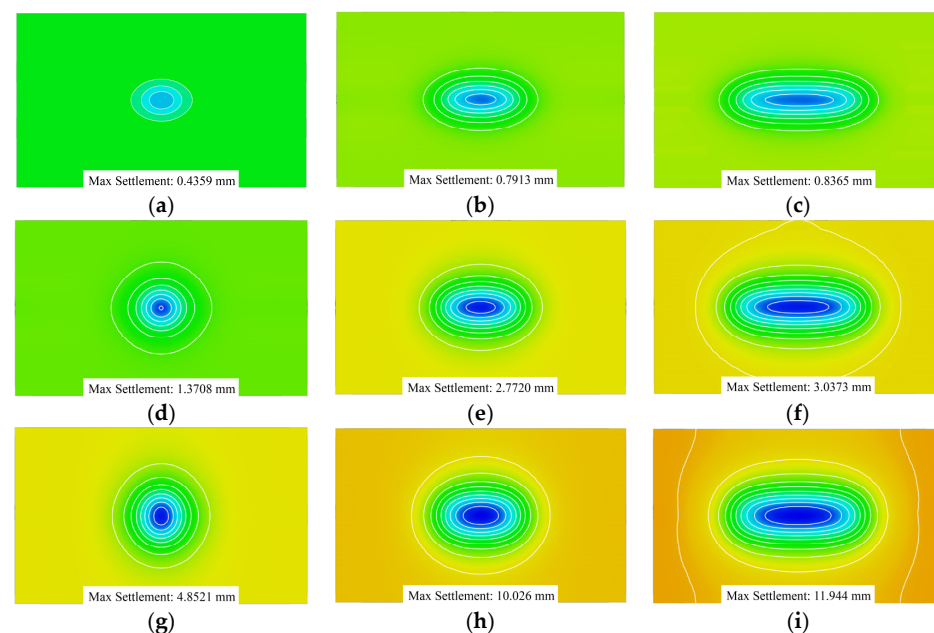


Figure 13. Calculation results of surface settlement caused by pipeline leakage under different conditions: (a) No. 1; (b) No. 2; (c) No. 3; (d) No. 4; (e) No. 5; (f) No. 6; (g) No. 7; (h) No. 8; (i) No. 9.

Furthermore, it shows that under the influence of the pipeline leakage, the surface settlement presents an elliptical distribution. The surface settlement range gradually increases with an increase in the pipeline leakage range and leakage length. In the same leakage range, with an increase in the leakage length, the surface settlement range mainly extends along the X-axis, whereas the Y-axis direction remains unchanged. However, for the same leakage length, with an increase in the leakage range, the surface settlement range mainly extends along the Y-axis direction, whereas the X-axis direction remains unchanged.

To further analyze the change rule of the affected area S and settlement value V with the leakage range and length, respective curves for S and V with the leakage range and length are shown in Figure 14.

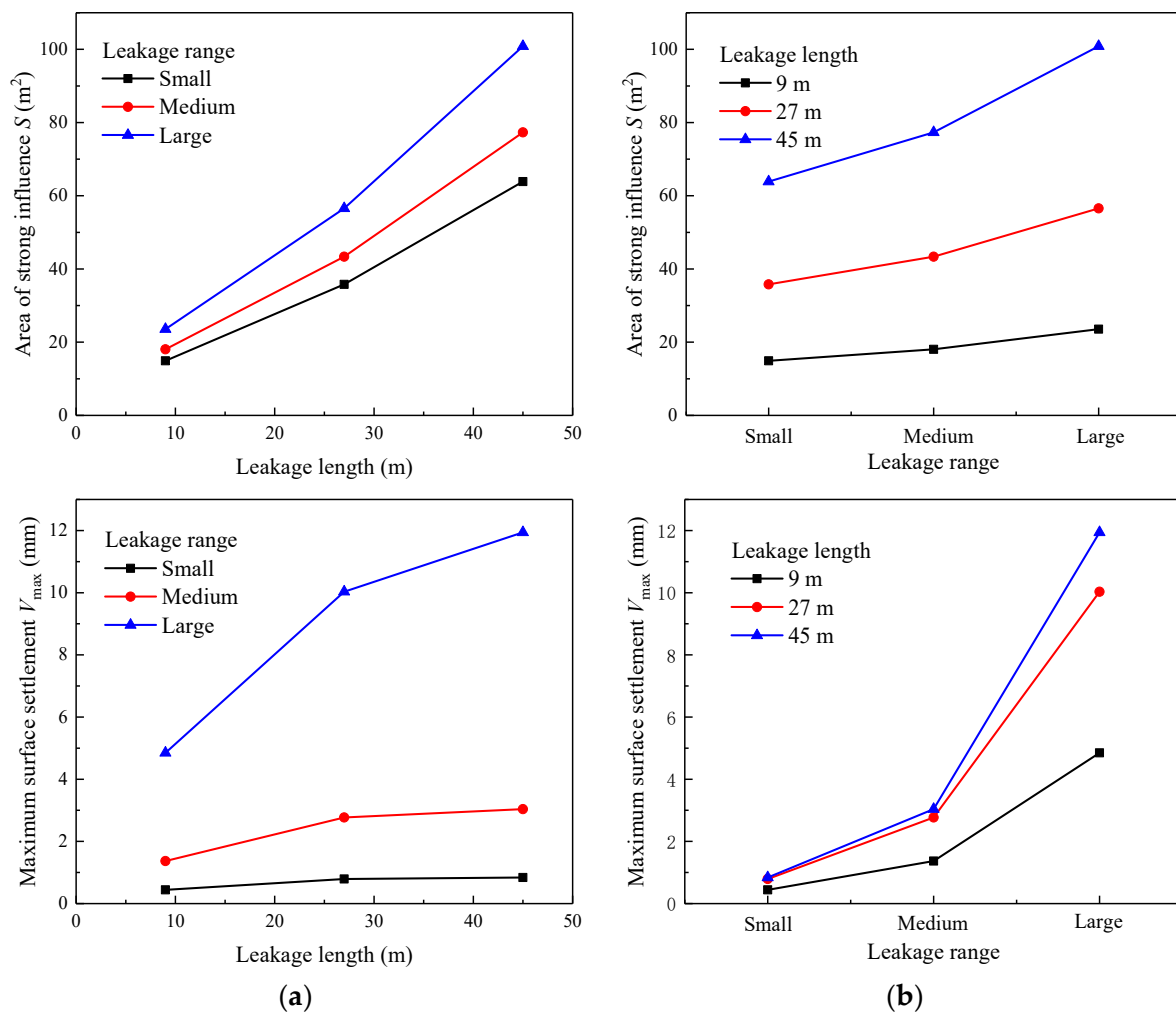


Figure 14. Variation of S and V with leakage range and leakage length: (a) the change rule of S and V with leakage length under different leakage ranges; (b) the change rule of S and V with leakage range under different leakage length.

Figure 14 shows that under the same leakage range, the strongly affected area S increases approximately linearly with an increase in leakage length. This means that with the increase of the leakage length, the scope of the strongly affected area increases linearly along the X-axis. At the same leakage length, S expands with the increase of leakage range, and its increment also gradually increases. This shows that the increase in the leakage range causes the surface settlement area to expand along the Y-axis. Under the joint influence of the leakage range and length, the increment of the strongly affected area gradually increases. The weak influence area has the same rule. In the same leakage range, the maximum surface settlement V_{max} increases with the expansion of the leakage length, and

its increment gradually decreases. This shows that the increase of the initial leakage along the X-axis has an evident effect on the settlement value, and that the maximum settlement value gradually stabilizes with the further increase of the leakage length. In addition, under the same leakage length, the increase of the leakage range has an evident impact on V_{\max} ; it makes V_{\max} increase exponentially, indicating that the leakage range is the main factor affecting the surface settlement.

To analyze the law of the ground settlement caused by the tunnel excavation under the influences of different leakage ranges and lengths, the shield construction of the left and right tunnels should be conducted immediately after the pipeline leakage reaches the preset range and length. Figure 15 shows the surface settlement curves after the completion of the left and right tunnels under different calculation conditions.

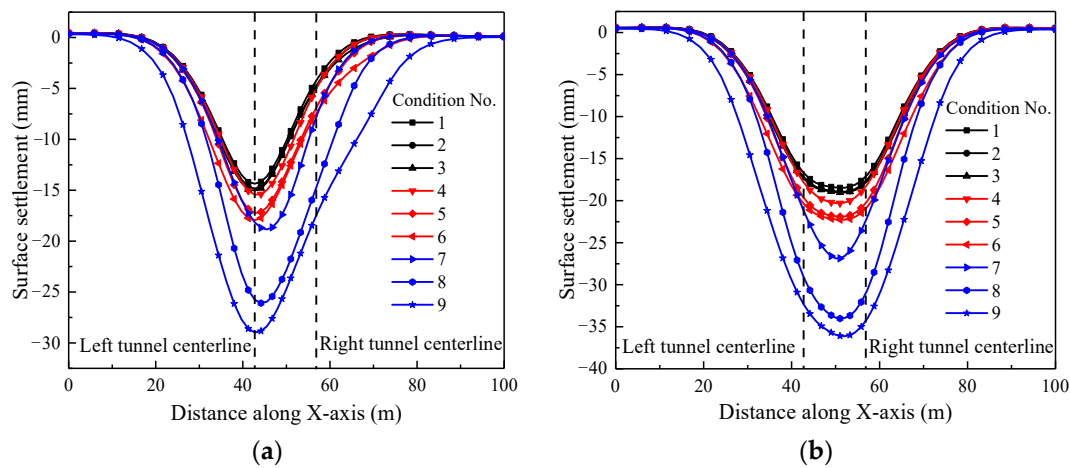


Figure 15. Surface settlement curve after twin tunnel construction under the influence of pipeline leakage: (a) single tunnel construction completed; (b) twin tunnel construction completed.

Figure 15 shows that under the influence of the pipeline leakage, the surface settlement caused by the tunnel excavation gradually increases with increases of the leakage range and leakage length. After the excavation of the left tunnel, the surface settlement mainly occurs just above the axis of the left tunnel. The maximum ground settlement under Condition 1 (small scope, leakage length of 9 m) is 14.4 mm, whereas that under Condition 9 (large scope, leakage length of 45 m) is 29 mm, nearly double. When the right tunnel is constructed, the maximum ground settlement will shift to the center line of the two tunnels. The maximum ground settlement under Condition 1 is 18.5 mm, and that under Condition 9 is 36.1 mm. This means that with increases in the leakage range and leakage length, the reduction of the soil strength between the pipeline and tunnel will significantly increase the ground settlement caused by the shield tunneling, especially with a large leakage range and length. This adverse effect cannot be ignored.

According to the nine monitoring points in the model, as shown in Figure 8, the soil displacement values after the construction of the left and right tunnels under different conditions were calculated and used to analyze the soil displacement change rule at different depths of the stratum, considering the influence of the seepage water.

Tables 7 and 8 indicate that with increases in the pipeline leakage range and leakage length, the soil displacements at different stratum depths increase after tunnel construction completion. As the measuring point was located on the vertical profile of the pipeline in the center of the stratum, the soil displacement at 3 m below the surface was slightly less than that at the surface, owing to the influence of the pipeline stiffness. This implies that the displacement of the soil above the pipeline decreases with an increase in depth. For the measuring point at a buried depth of 9.9 m, after the excavation of the left tunnel, the displacement value of the measuring point on axis 3 is the maximum, and those on axes 4

and 5 are the minimum. After the construction of the right tunnel, the displacement values of the measuring points of axes 3 and 5 are the largest, whereas that of axis 4 is the smallest.

Table 7. Displacement values of measuring points after completion of twin tunnel construction under different leakage ranges (the leakage length is 45 m, unit: mm).

Leakage Ranges	Depth of Measuring Points/m	Single Tunnel Construction Completed			Twin Tunnel Construction Completed		
		Axis 3	Axis 4	Axis 5	Axis 3	Axis 4	Axis 5
Small	0	−15	−9.7	−4.6	−17.4	−19	−17.7
	3	−14.6	−10.3	−4.4	−16.7	−18.7	−17.2
	9.9	−16.7	−5	−1.2	−17.7	−9.7	−18.1
Medium	0	−17.9	−13.5	−7.2	−20.4	−22.2	−20.7
	3	−17.4	−13.2	−6.9	−19.9	−21.6	−20.3
	9.9	−18.8	−4.9	−1.3	−21	−9.9	−21.5
Large	0	−29	−24.7	−17.1	−32.4	−36	−34
	3	−28.4	−24.2	−16.6	−31.3	−35.5	−33.4
	9.9	−31.1	−6.3	−1.4	−34.7	−11	−34.9

Table 8. Displacement values of measuring points after completion of twin tunnel construction under different leakage lengths (large-range leakage, unit: mm).

Leakage Lengths/m	Depth of Measuring Points/m	Single Tunnel Construction Completed			Twin Tunnel Construction Completed		
		Axis 3	Axis 4	Axis 5	Axis 3	Axis 4	Axis 5
9	0	−18.2	−16.5	−7.4	−21.2	−26.9	−21.9
	3	−17.3	−16.2	−6.9	−19.8	−26.4	−20.4
	9.9	−18.9	−4.5	−3	−21.3	−8.9	−22.2
27	0	−25.8	−22.8	−14.2	−29.1	−33.9	−30.6
	3	−25.2	−22.3	−14	−28.3	−33.4	−30
	9.9	−26.7	−5.4	−0.7	−30.2	−10.1	−31
45	0	−29	−24.7	−17.1	−32.4	−36	−34
	3	−28.4	−24.2	−16.6	−31.3	−35.5	−33.4
	9.9	−31.1	−6.3	−1.4	−34.7	−11	−34.9

This phenomenon can be explained by the superposition method, which is used to analyze the ground settlement law under the repeated disturbances of the twin tunnel during construction over a short distance. From the present research [30,31], the ground settlement mainly consists of the excavation settlement, consolidation settlement, and secondary consolidation settlement; of these, it is more necessary to consider the secondary consolidation settlement during tunnel operation. The ground losses caused by shield tunneling and soil reconsolidation caused by disturbances or shear failures around the tunnel are the fundamental reasons for ground settlement. Figure 16 shows a surface settlement trough caused by the excavation of the twin tunnel, where 1 is the surface settlement curve after the excavation of a single tunnel, S_{max} is the peak value of the surface settlement, R is the tunnel radius, D is the tunnel spacing, H is the tunnel burial depth, and β is the main influence angle of the tunnel excavation. Specifically, β represents the included angle between the line from the outer edge of the settlement trough to the bottom of the tunnel excavation outermost contour line and horizontal line. According to Table 7 and Figure 16, after the left tunnel is completed, all measuring points on axis 3 are located within the main influence angle range; therefore, the settlement value increases with the increase in depth. Two measuring points, E4 and B5, are located near the boundary line of the influence angle. If they are above the boundary line, the settlement value is higher than

that of the surface. In contrast, the settlement value gradually decreases with an increase in depth. After the construction of the left and right tunnels, the settlement values of the measuring points of axes 3 and 5 gradually increase with the depth. The settlement value of point E4 depends on the relative position of the monitoring point and point O. Therefore, the displacement change rule of each measuring point can be determined based on the layout depth of the measuring point and influence angle β . Based on the above analysis, combined with the soil displacements at different depths, as shown in Tables 7 and 8, it can be concluded that the influence of the leakage on the ground settlement is related to the amount of soil loss and disturbance degree. In the same stratum, the influence of a water leakage is greater in areas with strong disturbances and large soil losses.

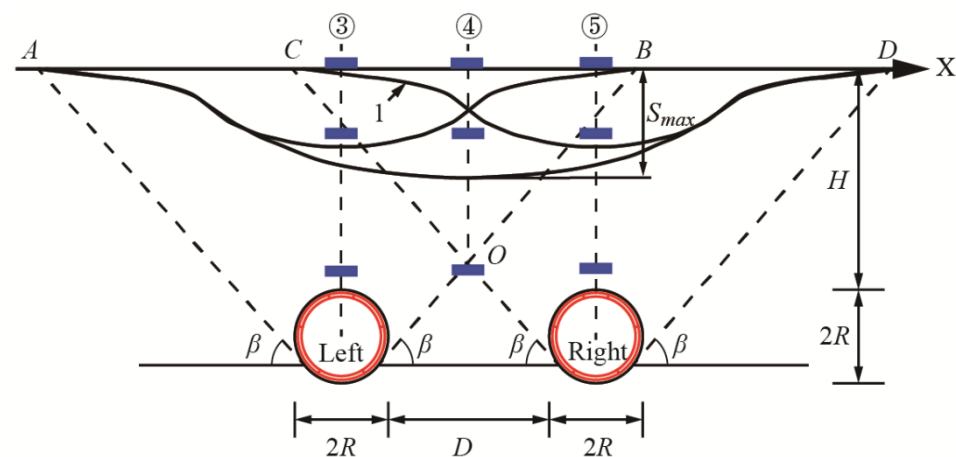


Figure 16. Surface settlement trough caused by the excavation of a twin tunnel.

6. Conclusions

This study was based on a tunnel project of Hefei Rail Transit Line 4, in China. First, a two-dimensional model was established to analyze the seepage diffusion law in the plane under the action of water pressure, and a three-dimensional finite element calculation model was constructed for the one-way coupling between the shield tunneling and pipeline leakage. The rationality of the model was verified by comparing it with the results from a model test and theoretical calculations. Finally, considering the influences of the diffusion range of the pipeline leakage along the stratum depth and leakage length along the pipeline direction, the change rule of the stratum settlement was analyzed, and the following conclusions were drawn.

- (1) The seepage water mainly diffuses vertically under the action of gravity. As the pipeline leakage gradually reaches the predetermined depth, the leakage diffusion range calculated by the numerical simulation tends to be consistent with that in the test results. However, owing to the existence of a large pore structure in the soil during the test, the leakage water is more likely to spread to the bottom of the pipeline under the action of gravity. Therefore, the error in the numerical simulation at the top of the pipeline is slightly larger than that at the bottom.
- (2) Under the condition that the pipeline does not leak, the theoretical solution is more accurate for predicting the excavation settlement of a single tunnel. In the calculations for twin tunnel excavation, the numerical simulation can consider the influence of repeated disturbances of the left and right tunnel construction, and is more accurate than the theoretical solution. Thus, the rationality of the three-dimensional calculation model is verified.
- (3) Through an influence analysis and calculation of the leakage parameters, it can be concluded that the surface settlement caused by pipeline leakage exhibits an elliptical distribution. Increases in the leakage length and scope cause the surface settlement

range to expand along the pipeline length and stratum depth, respectively. The maximum surface settlement increases with the expansion of the leakage length and leakage range, of which the leakage range is the main factor determining the maximum surface settlement.

- (4) For the soil displacement at different depths owing to the excavation of the double-track tunnel, the variation rule is determined by the arrangement depth of the measuring points and influence angle β . The influence of leakage on the formation settlement is related to the amount of soil loss and degree of disturbance. In the same stratum, the influence of the water leakage is greater in areas with strong disturbances and large soil losses.

Author Contributions: Conceptualization, X.S. and C.R.; methodology, X.S.; software, Y.C.; validation, G.A., H.W. and L.C.; formal analysis, C.R.; investigation, L.C.; resources, X.S.; data curation, Y.C.; writing—original draft preparation, X.S.; writing—review and editing, X.S.; visualization, Y.C.; supervision, C.R.; project administration, G.A.; funding acquisition, X.S. All authors have read and agreed to the published version of the manuscript.

Funding: This research was funded by the Scientific Research Foundation for High-level Talents of Anhui University of Science and Technology (2021yjrc12), Open Fund for Engineering Research Center of Underground Mine Construction, Ministry of Education (JYBGCZX2022106) and Science and Technology Planning Project of Housing Urban and Rural Construction in Anhui Province (2022-YF019).

Institutional Review Board Statement: Not applicable.

Informed Consent Statement: Not applicable.

Data Availability Statement: The data used to support the findings of this study are included within the manuscript.

Acknowledgments: Thanks to everyone who contributed to this article.

Conflicts of Interest: The authors declare no conflict of interest.

References

- Ni, P.; Mangalathu, S. Fragility analysis of gray iron pipelines subjected to tunneling induced ground settlement. *Tunn. Undergr. Space Technol.* **2018**, *76*, 133–144. [[CrossRef](#)]
- Shi, X.; Rong, C.; Cheng, H.; Cui, L.; Kong, J. An Energy Solution for Predicting Buried Pipeline Response Induced by Tunneling Based on a Uniform Ground Movement Model. *Math. Probl. Eng.* **2020**, *2020*, 1–12. [[CrossRef](#)]
- Yu, J.; Zhang, C.; Huang, M. Soil–pipe interaction due to tunnelling: Assessment of Winkler modulus for underground pipelines. *Comput. Geotech.* **2013**, *50*, 17–28. [[CrossRef](#)]
- Huang, M.; Zhou, X.; Yu, J.; Leung, C.; Tan, J.Q.W. Estimating the effects of tunnelling on existing jointed pipelines based on Winkler model. *Tunn. Undergr. Space Technol.* **2019**, *86*, 89–99. [[CrossRef](#)]
- Lin, C.G.; Huang, M.S.; Nadim, F.; Liu, Z. Tunnelling-induced response of buried pipelines and their effects on ground settlements. *Tunn. Undergr. Space Technol.* **2020**, *96*, 103193. [[CrossRef](#)]
- Lin, C.; Huang, M. Tunnelling-induced response of a jointed pipeline and its equivalence to a continuous structure. *Soils Found.* **2019**, *59*, 828–839. [[CrossRef](#)]
- Shi, J.; Wang, Y.; Ng, C.W. Numerical parametric study of tunneling-induced joint rotation angle in jointed pipelines. *Can. Geotech. J.* **2016**, *53*, 2058–2071. [[CrossRef](#)]
- Wham, B.P.; Argyrou, C.; O'Rourke, T.D. Jointed pipeline response to tunneling-induced ground deformation. *Can. Geotech. J.* **2016**, *53*, 1794–1806. [[CrossRef](#)]
- Shi, J.W.; Wang, Y.; Charles, W.W.N. Three-dimensional centrifuge modeling of ground and pipeline response to tunnel excavation. *J. Geotech. Geoenviron. Eng.* **2016**, *142*, 04016054. [[CrossRef](#)]
- Loganathan, N.; Poulos, H.G.; Stewart, D.P. Centrifuge model testing of tunnelling-induced ground and pile deformations. *Geotechnique* **2000**, *50*, 283–294. [[CrossRef](#)]
- Ma, S.; Shao, Y.; Liu, Y.; Jiang, J.; Fan, X. Responses of pipeline to side-by-side twin tunnelling at different depths: 3D centrifuge tests and numerical modelling. *Tunn. Undergr. Space Technol.* **2017**, *66*, 157–173. [[CrossRef](#)]
- Wu, J.; Jing, H.; Gao, Y.; Meng, Q.; Yin, Q.; Du, Y. Effects of carbon nanotube dosage and aggregate size distribution on mechanical property and microstructure of cemented rockfill. *Cem. Concr. Compos.* **2022**, *127*, 104408. [[CrossRef](#)]

13. Liu, X.; Zhang, Y.; Bao, Y. Full-scale experimental investigation on stagger effect of segmental tunnel linings. *Tunn. Undergr. Space Technol.* **2020**, *102*, 103423. [[CrossRef](#)]
14. Vorster, T.; Assaf, K.; Kenichi, S.; Mair, R.J. Estimating the effects of tunneling on existing pipelines. *J. Geotech. Geoenviron. Eng.* **2005**, *131*, 1399–1410. [[CrossRef](#)]
15. Saiyar, M.S.; Take, W.A.; Moore, I.D. Post-failure fracture angle of brittle pipes subjected to differential ground movements. *Tunn. Undergr. Space Technol.* **2015**, *49*, 114–120. [[CrossRef](#)]
16. Wang, Y.; Shi, J.; Ng, C.W. Numerical modeling of tunneling effect on buried pipelines. *Can. Geotech. J.* **2011**, *48*, 1125–1137. [[CrossRef](#)]
17. Shi, H.; Song, L.; Zhang, H.; Chen, W.; Lin, H.; Li, D.; Wang, G.; Zhao, H. Experimental and numerical studies on progressive debonding of grouted rock bolts. *Int. J. Min. Sci. Technol.* **2021**, *32*, 63–74. [[CrossRef](#)]
18. Hou, Y.; Fang, Q.; Zhang, D.; Wong, L.N.Y. Excavation failure due to pipeline damage during shallow tunnelling in soft ground. *Tunn. Undergr. Space Technol.* **2015**, *46*, 76–84. [[CrossRef](#)]
19. Zhang, C.; Zhu, J.; Huang, M.; Yu, J. Winkler load-transfer analysis for pipelines subjected to surface load. *Comput. Geotech.* **2019**, *111*, 147–156. [[CrossRef](#)]
20. Wu, J.; Feng, M.; Mao, X.; Xu, J.; Zhang, W.; Ni, X.; Han, G. Particle size distribution of aggregate effects on mechanical and structural properties of cemented rockfill: Experiments and modeling. *Constr. Build. Mater.* **2018**, *193*, 295–311. [[CrossRef](#)]
21. Zhang, J.; Xie, R. Numerical Analysis of Mechanical Behavior of Buried Pipes in Subsidence Area Caused by Underground Mining. *J. Press. Vessel Technol.* **2019**, *141*, 4042711. [[CrossRef](#)]
22. Cocchetti, G.; di Prisco, C.; Galli, A. Soil-pipeline interaction along unstable slopes; a coupled three-dimensional approach; Part 1, Theoretical formulation. *Can. Geotech. J.* **2009**, *46*, 1289–1304. [[CrossRef](#)]
23. Zhang, J.; Xie, R.; Zhang, H. Mechanical response analysis of the buried pipeline due to adjacent foundation pit excavation. *Tunn. Undergr. Space Technol.* **2018**, *78*, 135–145. [[CrossRef](#)]
24. Huang, Y.F.; Rong, C.X.; Shi, X. Experiment on the influence of soil suction and shear strength of unsaturated clay. *Sci. Tech. Eng.* **2021**, *21*, 10859–10866. (In Chinese)
25. Shi, X. Research on the Law of Ground Settlement and Pipeline Deformation under the Coupling Effect of Shield Construction and Adjacent Pipeline Leakage. Ph.D. Thesis, Anhui University of Science and Technology, Huainan, China, 2021. (In Chinese).
26. Yin, Z. An Experimental Study of the Relationships between Color, Degree of Saturation and Matrix Suction of Unsaturated Soils. Ph.D. Thesis, Tianjin University, Tianjin, China, 2014. (In Chinese).
27. Zhang, C.; Yue, Y.; Cai, Y. Influence of pipeline leakage range on ground deformation and failure during shallow tunnelling. *Chin. J. Rock Mech. Eng.* **2015**, *34*, 392–400. (In Chinese)
28. Shi, X.; Rong, C.; Cheng, H.; Cui, L.; Wang, B.; Sun, S. Analysis on Deformation and Stress Characteristics of a Multibraced Pit-in-Pit Excavation in a Subway Transfer Station. *Adv. Civ. Eng.* **2020**, *2020*, 1–19. [[CrossRef](#)]
29. Shi, X.; Rong, C.; Wang, H.; Cui, L.; Cai, H.; Wang, B. Analytical Study of Soil Displacement Induced by Twin Shield Tunneling in Semi-Infinite Viscoelastic Ground. *Adv. Civ. Eng.* **2020**, *2020*, 1–20. [[CrossRef](#)]
30. Wongsaroj, J.; Soga, K.; Mair, R. Tunnelling-induced consolidation settlements in London Clay. *Géotechnique* **2013**, *63*, 1103–1115. [[CrossRef](#)]
31. Cao, Y.; Jiang, J.; Xie, K.-H.; Huang, W.-M. Analytical solutions for nonlinear consolidation of soft soil around a shield tunnel with idealized sealing linings. *Comput. Geotech.* **2014**, *61*, 144–152. [[CrossRef](#)]